# Cronfa - Swansea University Open Access Repository

_____

This is an author produced version of a paper published in:
*Journal of Biomechanics*

_____

Cronfa URL for this paper:
http://cronfa.swan.ac.uk/Record/cronfa38961

_____

**Paper:**

Li, S., Wang, C. & Nithiarasu, P. (2018). Effects of the cross-linkers on the buckling of microtubules in cells. *Journal of Biomechanics*

http://dx.doi.org/10.1016/j.jbiomech.2018.03.002

_____

http://www.swansea.ac.uk/library/researchsupport/ris-support/

# Accepted Manuscript

Effects of the cross-linkers on the buckling of microtubules in cells

Si Li, Chengyuan Wang, Perumal Nithiarasu

# Effects of the cross-linkers on the buckling of microtubules in cells

Si Li, Chengyuan Wang[*], Perumal Nithiarasu

Zienkiewicz Centre for Computational Engineering, College of Engineering, Swansea University, Bay Campus, Fabian Way, Swansea, Wales SA1 8EN, UK

**Abstract** In cells, the protein cross-linkers lead to a distinct buckling behavior of microtubules (MTs) different from the buckling of individual MTs. This paper thus aims to examine this issue via the molecular structural mechanics (MSM) simulations. The transition of buckling responses was captured as the two-dimensional-linkers were replaced by the three-dimensional (3D) ones. Then, the effects of the radial orientation and the axial density of the 3D-linkers were examined, showing that more uniform distribution of the radial orientation leads to the higher critical load with 3D buckling modes, while the inhomogeneity of the axial density results in the localized buckling patterns. The results demonstrated the important role of the cross-linker in regulating MT stiffness, revealed the physics of the experimentally observed localized buckling and these results will pave the way to a new multi-component mechanics model for whole cells.

---

[*]Corresponding author. E-mail address: chengyuan.wang@swansea.ac.uk (C. Wang)

1

# 1. Introduction

Microtubules (MTs) are long protein polymer (Daneshmand et al., 2011), which maintain the cell stiffness/shapes, provide tracks for intracellular motility and facilitate other physiological processes (Howard and Hyman, 2003; Volokh et al., 2000). As MTs withstand compression in cells, buckling occurs for MTs (Brangwynne et al., 2006) and has attracted considerable attention from the community of cell mechanics (Bicek et al., 2009; Brangwynne et al., 2006; Heidemann et al., 1999; Sanchez et al., 2012).

The elastic beam models were employed to organize the experimental data (Felgner et al., 1996; Gittes et al., 1996; Kawaguchi et al., 2008; Takasone et al., 2002) and they provide an insight into the MT buckling (Brangwynne et al., 2006). The beam-like buckling was also reported for MTs in (Gao and Lei, 2009; Li, 2008). In 2006, an orthotropic shell model was proposed for MTs (Wang et al., 2006), and used in the analyses of MT buckling (Shen, 2010; Yi et al., 2008). Here, one of the observations is that MTs *in vivo* possess a critical buckling force ($F_{cr}$) higher than those *in vitro*. Attempts were then made to understand this in terms of the environmental effects, where cytoplasm of cells was simplified as an elastic media (Jiang and Zhang, 2008) (Li, 2008). Years later, a one-dimension (1D) finite element (FE) model was developed (Jin and Ru, 2013) where the cytoskeleton components around MTs were treated as discrete cross-linkers. This work provides the guidance to examine the role of the discrete cross-linkers in MT buckling (Hirokawa, 1982; Rodriguez et al., 2003) and offers a pathway to more realistic delineation of MT buckling *in vivo*.

Motivated by this study the present work is devoted to further studying localized MT buckling by using a three dimensional (3D) molecular structural mechanics (MSM) model (Zhang and Meguid,

2014; Zhang and Wang, 2014). The major issue examined is the effect of the spatial, random and inhomogeneous distributions of the proteinaceous linkers. Herein, the MSM and buckling realization were introduced in Section 2 followed by the validation of the model. The obtained results and discussions were given in Section 3, and the conclusions were drawn in Section 4.

## 2. Model development and validation

### 2.1 Model development

In this study, we considered 13-3 ($N$=13 $S$=3) MT of the most common configuration in *in vivo* situation (Chretien and Fuller, 2000; Chretien and Wade, 1991). As shown in Fig. 1, the space structure of MT was modeled as a framed MSM model, with the intra-PF bonds and inter-PF bonds modeled as elastic beams. The details of the MSM model for MT buckling simulation were explained in the supplementary material. The structure of the cross-linkers system supporting MTs laterally was depicted in Fig .1. All cross-linkers were modeled as springs with one end attached to the MT and the other end fixed to the surrounding media. The spring constant $k$ was taken as 39pN/nm (Peter and Mofrad, 2012) and the spatial density of the linkers was defined by the distance $L_d$ =100nm between the adjacent linkers for MT of length $L$=5μm. As the cross-linkers took axial tensile load with negligible compression (Bathe et al., 2008; Mehrbod and Mofrad, 2011), the spring modulus was set to be zero in compression. Herein, one MT end is clamped and the other is constrained by a roller. An axial compressive force was then applied to this roller end.

As shown in Fig. 1, a reference direction was picked up in the radial direction of an MT (dotted line) and the orientation of a radial linker was specified by measuring its angle $\delta_x$ relative to the

3

reference direction. The three-dimensional (3D) cross-linkers were then achieved by generating the linkers with $\delta_x$ randomly selected between 0° and 360° (anticlockwise positive). It is thus should be pointed out that, for 'MT-cross linker' systems considered in Secs.3.1 and 3.2, $L_d$, $L$ and $k$ remain the same but the randomly generated distribution of linker orientation varied from one system to another. The non-uniform linkers (Rodriguez et al., 2003) were also considered for MTs of length 10μm in Sec.3.3 where a part of the MT was supported by the dense-linkers ($L_d$ =25nm) and the rest was occupied by the low-density linkers ($L_d$ =200nm). The cross-linker spacing 25 to 200nm was observed in the experiments (Hirokawa, 1982; Svitkina et al., 1996) and later on, used in theoretical studies (Jin and Ru, 2013; Peter and Mofrad, 2012). The angle of adjacent linkers is fixed at 60°.

## 2.2 Validation of 3D MT model

Based on the MSM model, the length-dependent critical buckling load $F_{cr}$ was calculated for individual MTs and shown in Fig.2 in comparison with the experimental data obtained for *in vitro* MTs (Kikumoto et al., 2006) and an excellent agreement has been achieved.

Unfortunately, due to the uncertainty in *in vivo* condition, such a direct comparison cannot be made for the MT buckling supported by the cross-linkers. In spite of this, the MSM model predicted $F_{cr}$ of the order of 100 pN is comparable to the experimental data (Brangwynne et al., 2006) and theoretical results (Jiang and Zhang, 2008; Li, 2008). A more detailed comparison was made in Table 1 between the MSM model and the 1D-FE model accounting for the cross-linker effect (Jin and Ru, 2013). The MT length, constant density and elastic modulus of the linkers considered for the two models are exactly the same. Here, the MSM simulations considered the cross-linkers of 10 randomly generated orientation distributions. $F_{cr}$ achieved for the MT with the clamped-roller ends

4

fell in the range of [86.4pN, 294.3pN], quite close to [93pN, 353pN] given by the FE model for Clamped-Free and Clamped-Clamped ends. The localized mode shapes predicted by both models (Table 1) resemble those observed experimentally in (Brangwynne et al., 2006). In addition, the 3D MSM model captures the unique buckling mode observed in (Brangwynne et al., 2006), i.e., the 'localized buckling' at different places of MTs. The MT buckling with radial expansion was also achieved by the 3D MSM in Table 1 and Fig.3.

## 3. Results and discussions

In this section, the cross-linker model and the MSM model were employed to study the buckling of *in vivo* MTs, and examined the influence of the cross-linkers on MT buckling.

### 3.1 Transition due to the addition of the 3D-linkers

Herein, ten randomly generated cross-linker distributions were considered for the buckling of MT. The buckling modes of the MT-linker systems with the highest and lowest critical buckling load $F_{cr}$, were presented in Fig. 3. It was noticed that the randomly generated linkers lead to diverse buckling modes associated with significant variation in $F_{cr}$ values. It is thus of interest to examine the effect of the spatial cross-linkers.

To this end, we first considered 2D-linkers, which were parallelly aligned and distributed uniformly with a constant spatial density (Fig.4a). Subsequently, the 2D-linkers close to the clamped end were replaced by the 3D-linkers where the axial density remained unchanged but the radial orientations were randomly selected between 0 and 360° (Fig.4b). As shown in Fig. 4, the 2D-linkers

led to the planar bulking with one large half wave and the relatively low critical load $F_{cr}$ (Fig.4a). Addition of the 3D-linkers led to enhanced critical buckling load $F_{cr}$. When $\alpha$ (defined as the length covered by the 3D-linkers to MT length ratio) is not more than 30%, the buckled MTs still deform in the same plane (Fig. 4c) and $F_{cr}$ increased gradually with the rising amount of the 3D linkers. Once $\alpha$ was raised to 40%, the 2D beam-like buckling was transformed into 3D shell-like buckling, where radial expansion occurred and the central line of the shell became a 3D curved line (Fig. 4c). Associated with this change is the sudden growth of the buckling load $F_{cr}$ (from the order of $10pN$ to $100pN$) by one order of magnitude (Fig.4b). Further raising $\alpha$ above 40%, $F_{cr}$ of the 3D modes again increased progressively. These results given by the MSM model demonstrated the importance of the radial orientation of the cross-linkers in controlling the buckling behavior of MTs in cells.

## 3.2 Spatial distribution of the 3D-linkers

It is noted in our initial study that different critical buckling loads were achieved for the 'MT-3D cross-linker' systems where MT geometry, boundary conditions and the density of the cross-linkers were exactly the same. Obviously, the scattering of the obtained critical buckling load is due to the diverse spatial distributions generated randomly for the 3D-linkers. Thus, a more detailed study was conducted here to further examine the effect of the spatial distributions of the 3D cross-linkers. In doing this, we defined so-called '$n$-repeat' cross-linkers which comprise groups of 2D cross-linkers (Fig.5). The number of the cross-linkers $n$ remains the same for individual groups and the angle between adjacent two groups is 120° (Fig.5).

The critical buckling load $F_{cr}$ was then calculated in Fig. 5 for various MT-3D linker systems where the density $L_d$ varied from $25nm$ to $200nm$ and the number $n$ grew from 1 to 25. To

demonstrate the physical meaning of $n$ let us consider a system with MT length $175nm$ and $L_d$ = $25nm$. In this case, $n = 1$ gives pure 3D linkers where the angle between the adjacent linkers is 120°. Increasing $n$ to 4, we have the 3D linkers comprising 2 groups of 2D linkers (each has 4 linkers) and the angle between the two groups is again 120°. Further raising $n$ to 8 leads to 2D linkers. Thus, smaller $n$ led to the 3D linkers with more uniformly distributed orientation in circumferential direction.

It was found in Fig.5 that for the MT-3D linker systems considered, the highest $F_{cr}$ was obtained at $n = 1$, i.e., the MT is supported by the 3D-linkers with uniform distribution of the radial orientation. After this, $F_{cr}$ generally decreased with rising $n$. This observation indicated that less homogeneous distribution of the linker orientation usually down shifted the critical buckling load. This finding can shed some lights on the varying critical buckling loads achieved for the MT-cross linker systems with the same length and boundary conditions of MT, and the identical axial density of the cross-linkers. Furthermore, it was seen from Fig.5 that the effect of the cross-linker orientation turned out to be more significant for the MT-3D linker systems with the lower $L_d$ and smaller $n$. In addition, some exceptions were also found in Fig.5 where at $L_d = 25nm$ $F_{cr}$ associated with $n = 3$ was even higher than that associated with $n = 2$. The result suggested that other factors may also exert influence on MT buckling. For the MTs with 2D-linkers or individual MTs, it is well-known that $F_{cr}$ decreased with rising length. This common sense however may not be true for MTs supported by the 3D-linkers due to the effect of their spatial orientation.

## 3.3 Effect of the local dense 3D-linkers

The local dense-linkers are found in *in vivo* condition. A typical example is the dense actin network in the lamellipodia of cells (Rodriguez et al., 2003). To examine the effect of the local dense-linkers on MT buckling we considered the MT-linker systems with various sizes and locations of the dense-linkers having $L_d = 25nm$. The rest of the MT was supported by the low-density linkers with $L_d = 200nm$. The buckling modes and the associated buckling load were shown in Fig. 6 with the dense-linkers represented by the coarse lines. Here, buckling preferably occurred within the low-density linker regions showing the localized features of MT buckling. Such localized buckling close to the force applied tip (right side) was also achieved by the 1D-FE model (Jin and Ru, 2013). In the present simulations, buckling was also found in different places of MTs depending on the location of dense-linkers. These results agreed with the experimental observation and showed that experimentally observed '-deflected-straight-deflected-' MT buckling can be attributed to the local density variations of the surrounding cytoskeletal network (Brangwynne et al., 2006).

Furthermore, as disclosed in Fig.6a to 6h, $F_{cr}$ remained nearly constant when the distance was fixed between the right end of the dense-linkers and the loaded end of the MT (right side), although the length covered by the dense-linkers was varied by up to 3 times. During the calculations, the average density of the linkers was also changed substantially. The results thus suggested that the average linker density is not the key factor in controlling the buckling response in the cases considered. In contrast, the position of the right end of the dense-linkers or the length of the lower-density linkers between the local dense-linker and the loaded end of MTs (e.g., MT end close to the cell membrane) played an essential role in determining $F_{cr}$ of MTs in cells. Despite a few

8

exceptions, $F_{cr}$ exhibited a general trend to decrease from 133pN to 51pN when the right end of the dense-linkers moved towards the left, and the length of the low-density linkers close to the force applied end of MTs was increased by a factor of 6 (Fig. 6a to 6f). Specifically, in most cases the buckling of MTs was localized to the aforementioned region of the low-density linkers. Here it is worth mentioning that, in addition to the cross-linker thermal energy can also exert substantial influence on the buckling of MTs (Baczynski et al., 2007; Blundell and Terentjev, 2009; Hu et al., 2012; Lin et al., 2014). This issue thus deserves to be carefully examined in near future for MTs supported by the cross-linkers.

## 3. Conclusions:

The effects of the cross-linkers were examined for the buckling of MTs in cells with close connection established between the results and experimental data. The transition from planar buckling to 3D buckling was captured and the associated increase was observed in the critical buckling load due to the increase of the 3D-linkers. The 3D buckling modes were found to be in accordance with existing experimental observations.

For the 3D-linkers, the distribution of the radial orientation in the circumferential direction of MTs is identified as a determinant for MT buckling in cells. The more uniform radial distribution generally leads to a higher critical buckling load. Such an effect turns out to be more significant for the MTs supported by the 3D-linkers with higher density.

Another determinant of MT buckling is found to be the distribution of the linker density along

the axial direction of MTs. Inhomogeneous distribution gave rise to the localized MT buckling limited to the region of the low-density linkers. In particular, the critical load is very sensitive to the size variation of the low-density region close to the loaded end of MTs. The size of the dense-linker region and the average linker density, however, do not have a strong influence on MT buckling.

## Acknowledgments

## Conflicts of interest

There are no conflicts to declare.

## References

Baczynski, K., Lipowsky, R., Kierfeld, J., 2007. Stretching of buckled filaments by thermal fluctuations. Phys Rev E 76, 061914.

Bathe, M., Heussinger, C., Claessens, M.M., Bausch, A.R., Frey, E., 2008. Cytoskeletal bundle mechanics. Biophys. J. 94, 2955-2964.

Bicek, A.D., Tüzel, E., Demtchouk, A., Uppalapati, M., Hancock, W.O., Kroll, D.M., Odde, D.J., 2009. Anterograde microtubule transport drives microtubule bending in LLC-PK1 epithelial cells. Mol. Biol. Cell 20, 2943-2953.

Blundell, J., Terentjev, E., 2009. Buckling of semiflexible filaments under compression. Soft Matter

5, 4015-4020.

Brangwynne, C.P., MacKintosh, F.C., Kumar, S., Geisse, N.A., Talbot, J., Mahadevan, L., Parker, K.K., Ingber, D.E., Weitz, D.A., 2006. Microtubules can bear enhanced compressive loads in living cells because of lateral reinforcement. J. Cell Biol. 173, 733-741.

Chretien, D., Fuller, S.D., 2000. Microtubules switch occasionally into unfavorable configurations during elongation. J. Mol. Biol. 298, 663-676.

Chretien, D., Wade, R.H., 1991. New data on the microtubule surface lattice. Biol. Cell. 71, 161-174.

Daneshmand, F., Ghavanloo, E., Amabili, M., 2011. Wave propagation in protein microtubules modeled as orthotropic elastic shells including transverse shear deformations. J. Biomech. 44, 1960-1966.

Felgner, H., Frank, R., Schliwa, M., 1996. Flexural rigidity of microtubules measured with the use of optical tweezers. J. Cell Sci. 109, 509-516.

Gao, Y.W., Lei, F.-M., 2009. Small scale effects on the mechanical behaviors of protein microtubules based on the nonlocal elasticity theory. Biochem. Biophys. Res. Commun. 387, 467-471.

Gittes, F., Meyhöfer, E., Baek, S., Howard, J., 1996. Directional loading of the kinesin motor molecule as it buckles a microtubule. Biophys. J. 70, 418-429.

Heidemann, S.R., Kaech, S., Buxbaum, R.E., Matus, A., 1999. Direct Observations of the Mechanical Behaviors of the Cytoskeleton in Living Fibroblasts. The J. Cell. Biol. 145, 109-122.

Hirokawa, N., 1982. Cross-linker system between neurofilaments, microtubules and membranous organelles in frog axons revealed by the quick-freeze, deep-etching method. The J. Cell. Biol. 94, 129.

Howard, J., Hyman, A.A., 2003. Dynamics and mechanics of the microtubule plus end. Nature 422, 753-758.

Hu, B., Shenoy, V.B., Lin, Y., 2012. Buckling and enforced stretching of bio-filaments. Journal of the Mechanics and Physics of Solids 60, 1941-1951.

Jiang, H., Zhang, J., 2008. Mechanics of microtubule buckling supported by cytoplasm. Journal of Applied Mechanics 75, 061019.

Jin, M.Z., Ru, C.Q., 2013. Localized buckling of a microtubule surrounded by randomly distributed cross linkers. Phys Rev E 88, 012701.

Kawaguchi, K., Ishiwata, S.i., Yamashita, T., 2008. Temperature dependence of the flexural rigidity of single microtubules. Biochem. Biophys. Res. Commun. 366, 637-642.

Kikumoto, M., Kurachi, M., Tosa, V., Tashiro, H., 2006. Flexural rigidity of individual microtubules measured by a buckling force with optical traps. Biophys. J. 90, 1687-1696.

Li, T., 2008. A mechanics model of microtubule buckling in living cells. J. Biomech. 41, 1722-1729.

Lin, Y., Wei, X., Qian, J., Sze, K.Y., Shenoy, V.B., 2014. A combined finite element-Langevin dynamics (FEM-LD) approach for analyzing the mechanical response of bio-polymer networks. Journal of the Mechanics and Physics of Solids 62, 2-18.

Mehrbod, M., Mofrad, M.R., 2011. On the significance of microtubule flexural behavior in cytoskeletal mechanics. PLoS One 6, e25627.

Peter, S.J., Mofrad, M.R., 2012. Computational modeling of axonal microtubule bundles under tension. Biophys. J. 102, 749-757.

Rodriguez, O.C., Schaefer, A.W., Mandato, C.A., Forscher, P., Bement, W.M., Waterman-Storer,

12

C.M., 2003. Conserved microtubule–actin interactions in cell movement and morphogenesis. Nat. Cell Biol. 5, 599-609.

Sanchez, T., Chen, D.T., DeCamp, S.J., Heymann, M., Dogic, Z., 2012. Spontaneous motion in hierarchically assembled active matter. Nature 491, 431-434.

Shen, H.S., 2010. Nonlocal shear deformable shell model for postbuckling of axially compressed microtubules embedded in an elastic medium. Biomech Model Mechanobiol 9, 345-357.

Svitkina, T.M., Verkhovsky, A.B., Borisy, G.G., 1996. Plectin sidearms mediate interaction of intermediate filaments with microtubules and other components of the cytoskeleton. The J. Cell. Biol. 135, 991-1007.

Takasone, T., Juodkazis, S., Kawagishi, Y., Yamaguchi, A., Matsuo, S., Sakakibara, H., Nakayama, H., Misawa, H., 2002. Flexural rigidity of a single microtubule. Jpn. J. Appl. Phys. 41, 3015.

Volokh, K.Y., Vilnay, O., Belsky, M., 2000. Tensegrity architecture explains linear stiffening and predicts softening of living cells. J. Biomech. 33, 1543-1549.

Wang, C.Y., Ru, C.Q., Mioduchowski, A., 2006. Orthotropic elastic shell model for buckling of microtubules. Phys. Rev. E Stat. Nonlin. Soft Matter Phys. 74, 052901.

Yi, L., Chang, T., Ru, C., 2008. Buckling of microtubules under bending and torsion. J. Appl. Phys. 103, 103516.

Zhang, J., Meguid, S., 2014. Buckling of microtubules: An insight by molecular and continuum mechanics. Appl. Phys. Lett. 105, 173704.

Zhang, J., Wang, C.Y., 2014. Molecular structural mechanics model for the mechanical properties of microtubules. Biomech. Model. Mechan. 13, 1175-1184.

13

## Table and caption

Table 1 Comparison to the cross-linked 1D-FE model

| MTs | FEM(Jin and Ru, 2013) | MSM |
|---|---|---|
| Length | 5μm | |
| Cross-linkers | $L_d$=100nm; $k$=39pN/nm | |
| Critical buckling force and buckling mode shape | | |
| *B. C. | Clamped-Free | Clamped-Roller |
| $F_{cr}$ | 93.0 pN | 86.4-294.3 pN |
| Mode shape |  |  |
| B. C. | Clamped-Clamped | |
| $F_{cr}$ | 353.0 pN | |
| Mode shape |  |  |

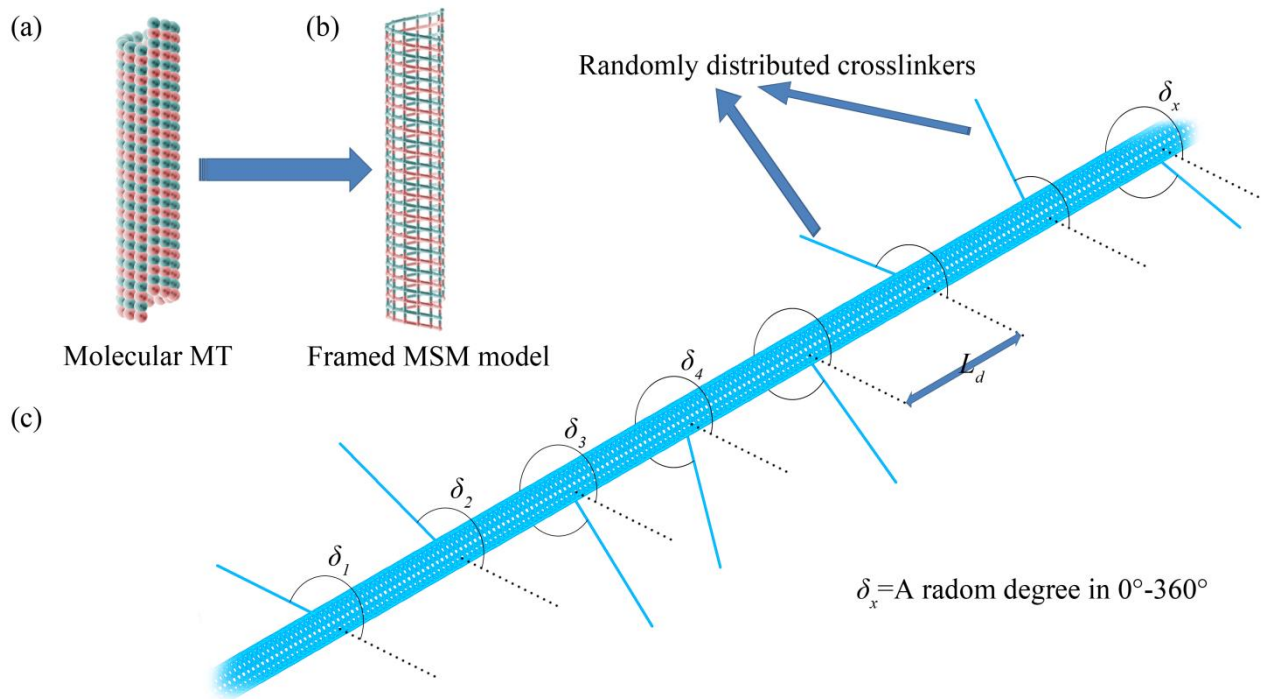* B. C.: boundary condition

# Figures and captions



Fig. 1 (a) Structural representation of an MT, (b) the MSM model and (c) the structure of the cross-linker system supporting MTs.
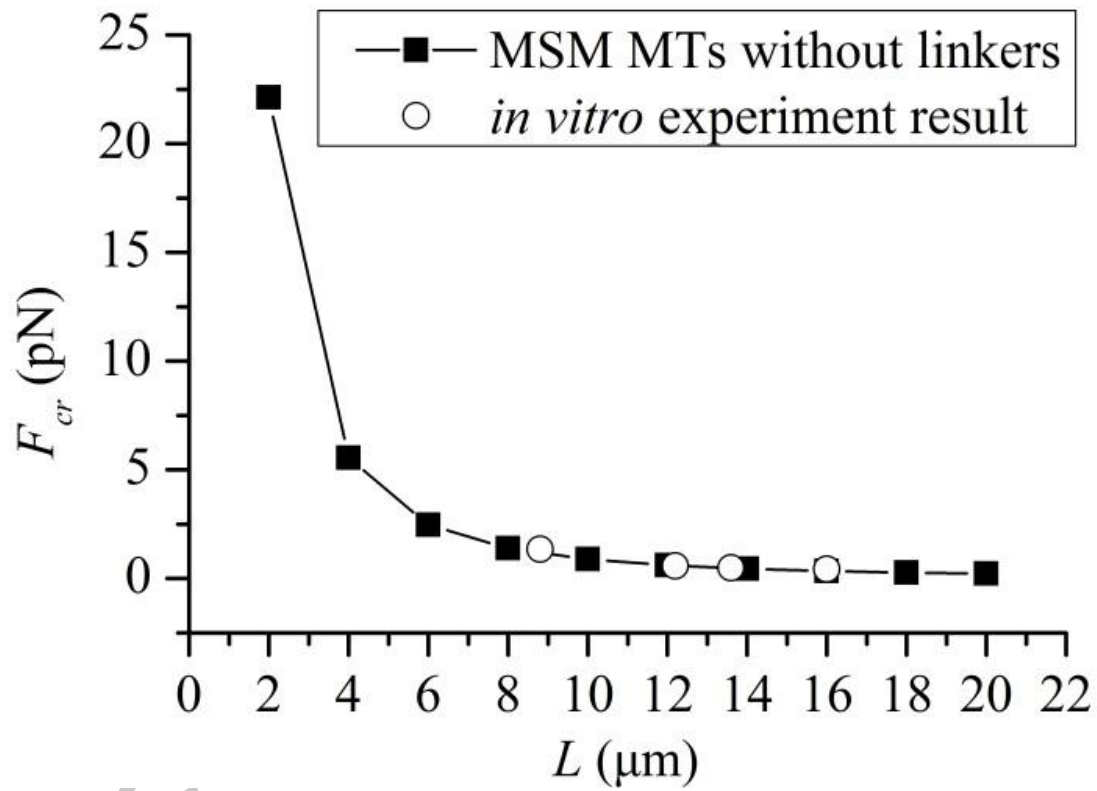
Fig. 2 The length-dependent $F_{cr}$ calculated for individual MTs in comparison with the experimental
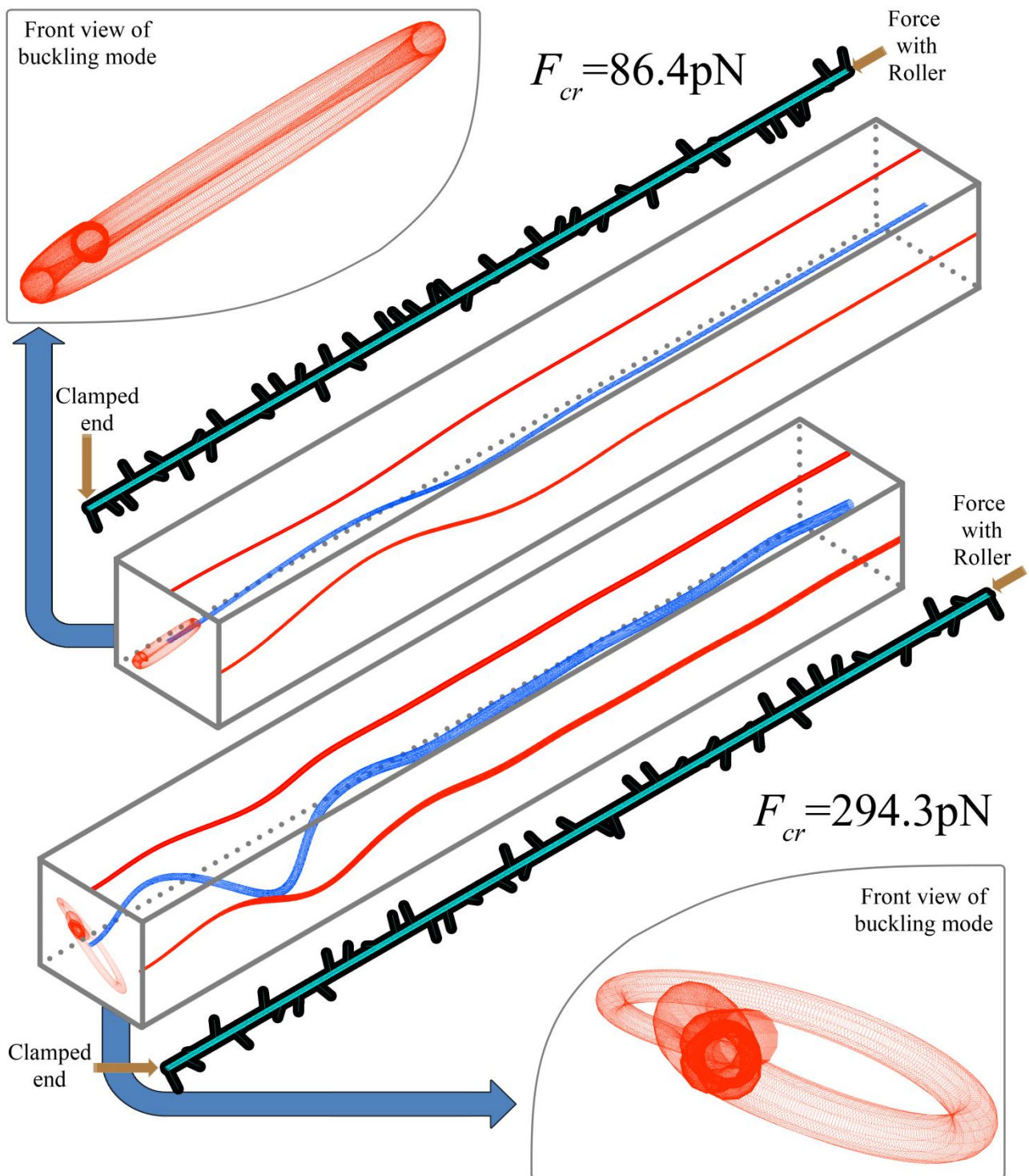
data

Front view of buckling mode

$F_{cr}$=86.4pN

Force with Roller

Clamped end

Force with Roller

$F_{cr}$=294.3pN

Front view of buckling mode

Clamped end

Fig. 3 The 3D bulkling modes of the selected MT-linker systems with randomly generated cross-linkers.

(a)

2D- linked model
(Right view)

7.49 pN

(b)

10 % 3D linked

20 % 3D linked

Clamped end

| | $F_{cr}$ (pN) | | | |
|---|---|---|---|---|
| 0% | 10% | 20% | 30% | 40% |
| 7.49 | 7.50 | 9.66 | 12.83 | 115.16 |
| 50% | 60% | 70% | 80% | 90% |
| 110.73 | 151.94 | 117.95 | 132.29 | 131.00 |

(c)

Right view

30%                                          40%

Front view (after rotation)
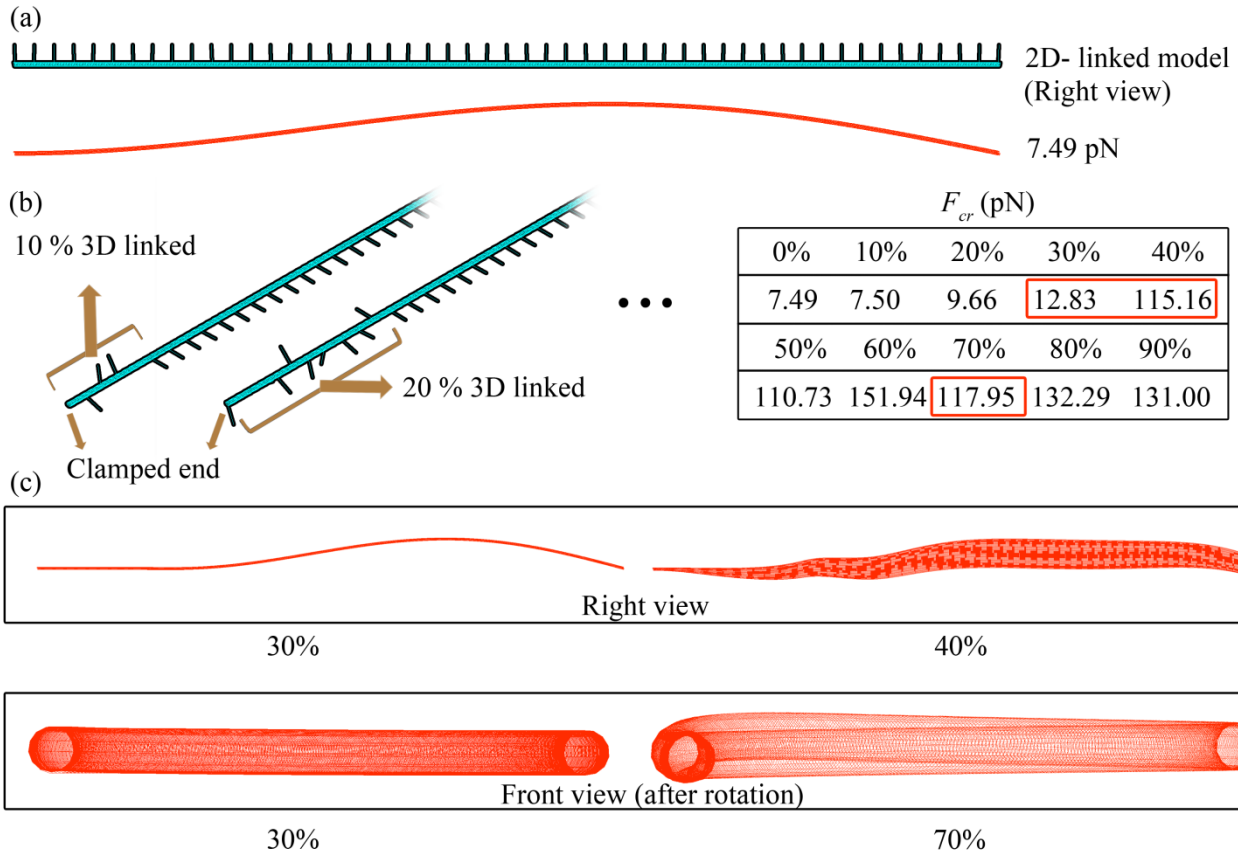
30%                                          70%

Fig. 4 The effect of the spatial linker orientations obtained by considering a 2D-linker system and the systems with increasing amount of the 3D-linkers.
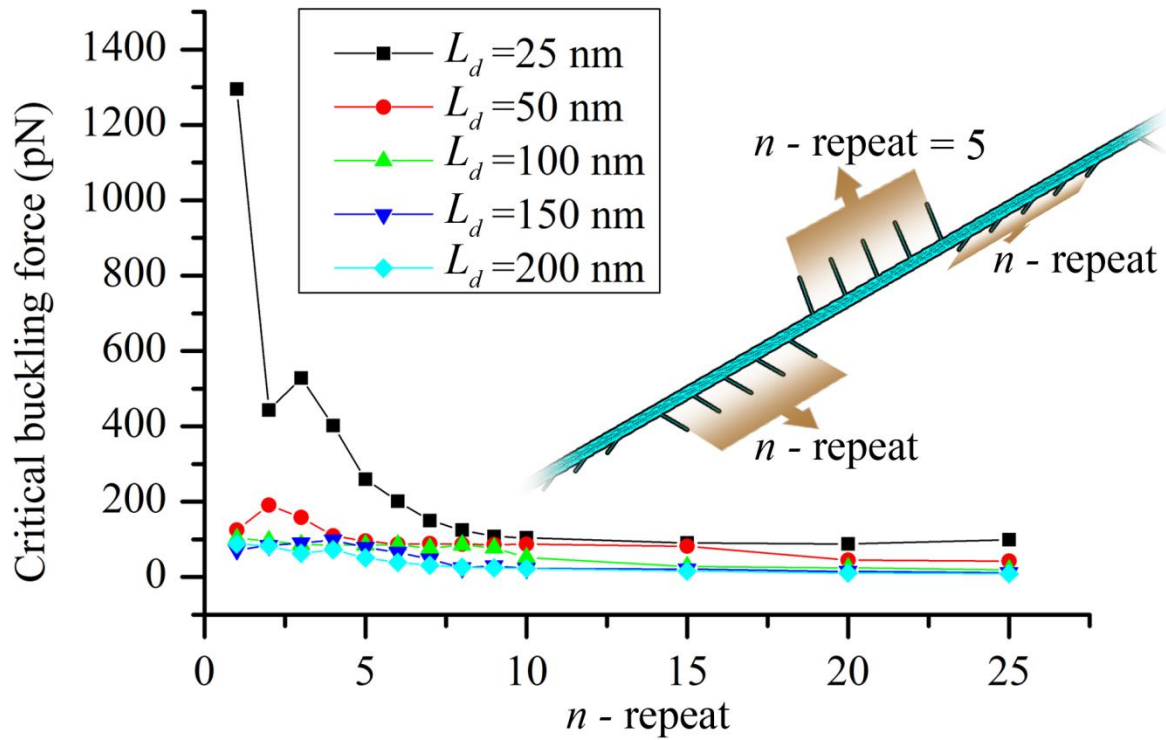
Fig. 5 The effect of the spatial linker distributions on the critical buckling load obtained by considering the 'n-repeat' linkers

The portion of MT modeled with dense linkers ($L_d$=25 nm)

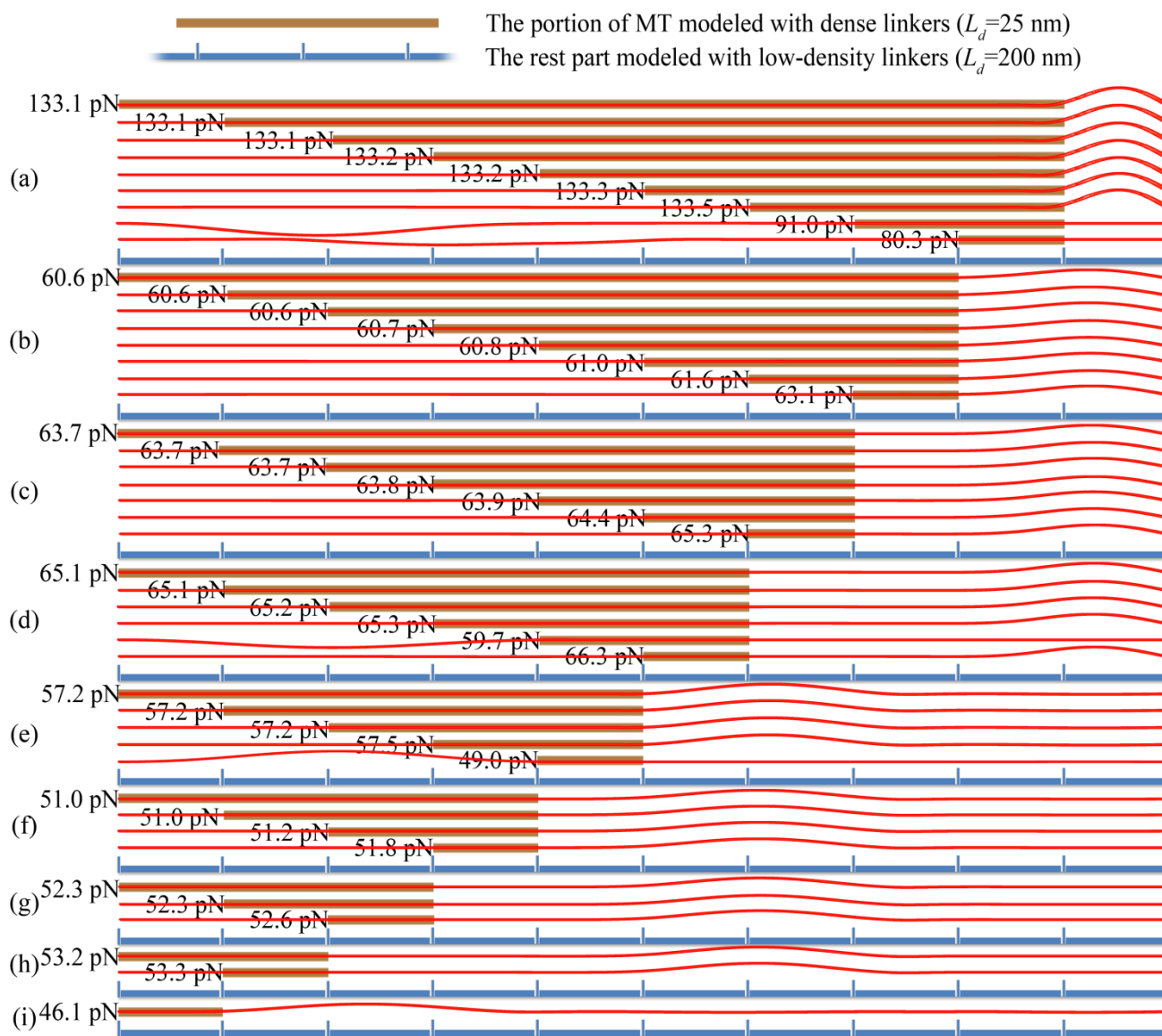The rest part modeled with low-density linkers ($L_d$=200 nm)

Fig. 6 The effect of the local dense linkers on the buckling modes and associated critical loads.